Proceedings of Australasian Conference on Robotics and Automation, 3-5 Dec 2012, Victoria University of Wellington, New Zealand.

Dynamic Modelling and Analysis of a Vectored Thrust Aerial Vehicle

Wei Yuan, Hiranya Jayakody and Jay Katupitiya
School of Mechanical and Manufacturing Engineering,
University of New South Wales, Sydney, Australia
{w.yuan@unsw,j.katupitiya@unsw,hiranya.jayakody@student}.unsw.edu.au

Abstract

This paper presents the dynamic modelling of a Vectored Thrust Aerial Vehicle (VTAV) powered by ducted fans, some of which can be vectored. First, a comprehensive nonlinear dynamic model of the system is developed. The model is then linearized around the hover equilibrium and the characteristics of the linearized model is analyzed. The performance of the linearized model is compared with the nonlinear model for various test conditions in order to identify the important parameters that need to be taken into consideration in developing a robust controller for the VTAV.

1 Introduction

Research in to Micro Aerial Vehicles (MAV) has increased significantly in the past several decades due to their applicability in various civil and military applications. Features such as Vertical Take Off and Landing (VTOL) capability has further enhanced the use of MAVs in congested environments where the vehicle has little space for take-off and landing[Marconi *et al.*, 2011].

MAVs are developed based on open propellers [Liu *et al.*, 2009] such as coaxial helicopters and quad rotors, as well as ducted fanned systems [Naldi *et al.*, 2010]. Among the two categories ducted fan based aerial vehicles have many advantages that deserve a greater attention than has been to date. Ducted fans provide safe operation in cluttered environments where the objects in the proximity of the vehicle are protected from the propeller and vice versa. Further, the ducted fanned systems exhibit better overall efficiency at low speeds, due to the reduction of blade tip losses as well as predefined uniform cross section. Other advantages unique to the design presented in this paper are discussed below.

The majority of the research aimed at ducted fanned systems are based on single ducted fan platforms such as iStar9, HoverEye, AROD, GTSpy with a fuselage and control surfaces mounted beneath the ducted propeller [Johnson and Turbe, 2006] [Pflimlin *et al.*, 2010]. However these types of single ducted fan systems show large pitch and roll movements during forward flight [Omar *et al.*, 2008] which is highly undesirable in applications like terrain mapping using a sensor payload. Furthermore, these types of vehicles are unable to carry a large payload due to their design limitations. Quad-rotor platforms on the other hand provides payload carrying capacity yet need to undergo roll and pitch movements for forward and sideways flight [Bai *et al.*, 2011]. Designs similar to the aerial vehicle discussed in this paper which includes multiple ducted fans with vectoring are rare. Due to its vectoring capability, this MAV is known as a Vectored Thrust Aerial Vehicle (VTAV) [Kumon *et al.*, 2010]. The VTAV overcomes the above mentioned disadvantages of the existing MAVs through its unique design. The VTAV which has a triangular shape consists of three ducted fans as shown in Figure 1. The rear two ducted fans can be vectored or turned about an axis common to both ducted fans. The independent vectoring of these two fans allows the yaw motion and forward flight with minimal or no pitch movement. As will be seen, the dynamic model demonstrates unstable equilibrium and is significantly simpler than the dynamic model of a helicopter. The fact that the system is in unstable equilibrium also allows us to develop control systems that will provide greater maneuverability than would have been possible with quad-rotor

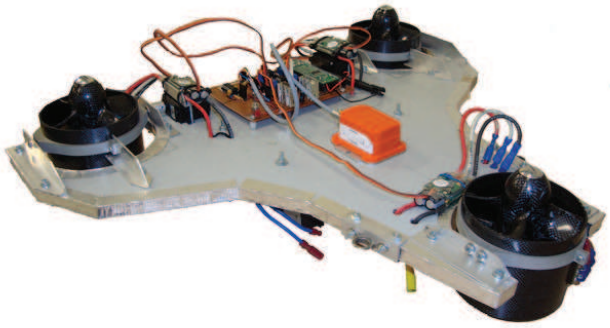

Figure 1: Vectored Thrust Aerial Vehicle (VTAV)

systems or co-axial helicopters. Unlike single ducted fan systems, this design provides ample space for a sizable payload bay. Minimal pitch and roll movements ensure that the VTAV is suitable to carry vision sensors and laser range sensors for terrain mapping where the attitude of the sensors play a major role on the reliability of acquired data.

The aim of this paper is to provide a comprehensive nonlinear dynamic model of this unique platform considering all forces affecting the VTAV. The dynamic nonlinear MIMO model is then linearized at the hover condition. The characteristics of the linearized model is discussed while providing an insight in to multivariable system stability and frequency response and parameters which play an important role in designing a controller for the VTAV. Finally the dynamic response of the linearized model is compared with the nonlinear model for various operational conditions, to validate the use of linearized model in place of the nonlinear model, in designing controllers.

2 VTAV System Description

The VTAV platform takes the shape of a regular triangle with three fans mounted at each vertex of the triangle. The axis of the front ducted fan is fixed perpendicular to the plane of the triangle, whilst the rear two fans are able to rotate around an axis which is common to both fans as shown in Figure 2. The lightweight honeycomb body of the VTAV enables it to carry a heavier payload. The control inputs to the system are the three fan speeds and the two vectoring angles.

All motors on the VTAV are powered by Li-Ion batteries. The low level controllers are implemented in an onboard micro-controller that commands the motors via electronic speed controllers. A wireless device attached to the onboard micro-controller enables the VTAV to send and receive data to/from a ground station. The accelerations, gyro rates and the GPS positions of the VTAV are measured using an onboard inertial sensor.

3 Dynamic Modelling

The VTAV described in Section 2 is subjected to various forces and moments. It is important to transform these forces and moments to a common reference frame so that the derived system model is independent of the attitude and heading of the VTAV at any given time. Therefore, three coordinate frames I,B and D are introduced to model the forces and moments acting upon the VTAV.

3.1 Coordinate Frames

The inertial coordinate frame is denoted by I with the vector basis (x_0 y_0 z_0) with x_0 pointing towards North, z_0 pointing towards the center of Earth and y_0 completing a right handed coordinated system. Coordinate frame B is attached to the body of the VTAV. The vector basis is denoted by (x_b y_b z_b) with its origin being the center of gravity of the vehicle. As shown in Figure 2, x_b points forwards, z_b points downwards and y_b is set such that is completes a right handed coordinate frame.

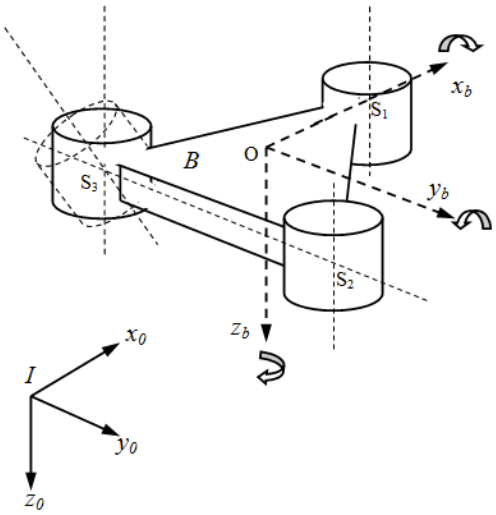

Figure 2: VTAV model and coordinate frames layout

Coordinate frame D with the vector basis (x_d y_d z_d) is associated with each of the rear ducted fans of the VTAV. In frame D, y_d is set along the axis of vectoring of the ducted fan and z_d is set along the axis of rotation of the fan. x_d completes a right handed coordinate system as shown in Figure 3.

Rotational matrices with roll, pitch and yaw Euler angles are then introduced to transform the forces to a common coordinate frame; in this case the VTAV body frame. The rotational matrix R, which is also the transformation matrix from B to I can be described using the Euler angles Φ, Θ, Ψ as follows.

$$R = \begin{pmatrix} c_\Theta c_\Psi & s_\Theta s_\Phi c_\Psi - s_\Psi c_\Phi & s_\Theta c_\Phi c_\Psi + s_\Psi s_\Phi \\ c_\Theta s_\Psi & s_\Theta s_\Phi s_\Psi + c_\Psi c_\Phi & s_\Theta c_\Phi s_\Psi - c_\Psi s_\Phi \\ -s_\Theta & c_\Theta s_\Phi & c_\Theta c_\Phi \end{pmatrix} \quad (1)$$

In (1) c ans s represent cosine and sine functions respectively. Similarly the rotational matrix from I to B would be R^T.

Given the vectoring angle for a rear motor as θ_d the rotational matrix from B to D can be described as,

$$R_d = \begin{pmatrix} c_{\theta_d} & 0 & -s_{\theta_d} \\ 0 & 1 & 0 \\ s_{\theta_d} & 0 & c_{\theta_d} \end{pmatrix} \quad (2)$$

3.2 Newton-Euler Equations

The VTAV can be considered as a rigid body. Therefore the forces and torques acting on the VTAV are

governed by the Newton-Euler equations as described below [Wang *et al.*, 2007].

$$m\dot{v}_b + m(\omega_b \times v_b) = F_b, \tag{3}$$

$$J_b\dot{\omega}_b + (\omega_b \times J_b\omega_b) = M_b, \tag{4}$$

where F_b and M_b represent the total force and moment vectors acting on the VTAV body, m is the mass of the vehicle and J_b represents the moment of inertia of the vehicle. J_b is denoted as,

$$J_b = \begin{pmatrix} I_{xx} & 0 & 0 \\ 0 & I_{yy} & 0 \\ 0 & 0 & I_{zz} \end{pmatrix}. \tag{5}$$

The terms v_b=$[v_{bx}\ v_{by}\ v_{bz}]^T$ and ω_b=$[\omega_{bx}\ \omega_{by}\ \omega_{bz}]^T$ represent the velocities and angular speeds of the VTAV with respect to the body frame, respectively.

3.3 Forces

Gravitational acceleration in the Inertial frame I can be represented as, G_I=$[0,\ 0,\ g]^T$

Therefore the gravitational pull acting upon the VTAV with respect to the body frame yields,

$$G^b = mR^T G_I. \tag{6}$$

The thrust forces generated by the ducted fans are the forces that enable the VTAV to fly. The relationship between the generated thrust T and the angular velocity ω_f of the motor can be approximated by [Pflimlin *et al.*, 2010],

$$T = C_t\omega_f^2, \tag{7}$$

where C_t is a constant that depends on the propeller diameter, thrust coefficient of the propeller and the air density [Naldi *et al.*, 2010]. As the total thrust force is directed along the z_d direction, the thrust generated by a single fan w.r.t. the duct frame D can be described as,

$$F_{Td} = \begin{pmatrix} 0 \\ 0 \\ -T \end{pmatrix}. \tag{8}$$

Therefore the thrust force on the body frame is,

$$F_{Tb} = R_d^T F_{Td}. \tag{9}$$

The two main forces which adversely affect the operation of a ducted fan can be identified as the ram drag and the momentum drag. Drag forces occur due to the relative airflow with respect to the duct, when the ducted fan forces the air outside its inlet to flow through the duct in order to generate thrust. Ram drag occurs due to the relative airflow perpendicular to the duct axis, z_d, and can be modeled as,

$$D_r = C_d\omega_f v_{r_{xy}}, \tag{10}$$

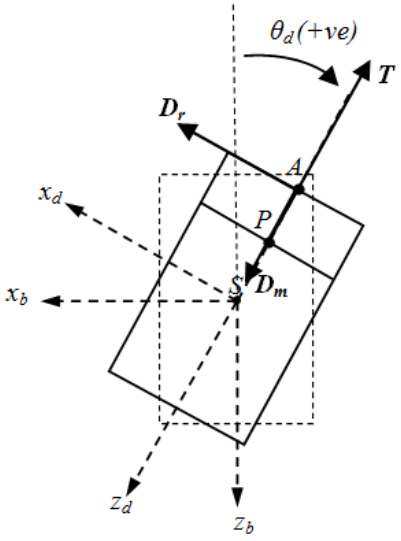

Figure 3: Forces acting on a single duct. T-Thrust Dr-Ram Drag Dm-Momentum Drag

where C_d is a constant coefficient and $v_{r_{xy}}$ is the relative air velocity perpendicular to the duct axis, z_d [Ko *et al.*, 2007]. Momentum drag acts along the z_d axis against the generated thrust force, when there is a relative air velocity with respect to the duct axis. The momentum drag force which is quite small when compared to the generated thrust force is often neglected in modeling of micro aerial vehicles. However, in order to develop a complete model, momentum drag is also taken into consideration. Momentum drag , D_m, can be modeled as,

$$D_m = C_m v_{r_z}^2, \tag{11}$$

where C_m is a constant coefficient and v_{r_z} is the relative air velocity along the duct axis z_d [Pflimlin *et al.*, 2010]. Sudden wind gusts are also capable of creating and affecting the existing drag forces on the vehicle. If the wind velocity in the inertial frame is given as W_i =$[W_{ix}\ W_{iy}\ W_{iz}]^T$ the relative airflow against the body of the VTAV can be described as,

$$v_{br} = R^T W_i - v_b \tag{12}$$

Therefore the relative wind vector acting on the duct would be,

$$v_r = R_d v_{br}, \tag{13}$$

and the total drag force would be,

$$F_{Dd} = \begin{pmatrix} C_d\omega_f v_{rx} \\ C_d\omega_f v_{ry} \\ C_m v_{rz}^2 \end{pmatrix}. \tag{14}$$

As a result, the resultant drag force on the body frame is,

$$F_{Db} = R_d^T F_{Dd} \tag{15}$$

The drag forces occur at the center of pressure A, located on the z_d axis at the duct lip. Although there is

a possibility that the location of point A may vary depending on the angle of attack of wind and vectoring of ducted fans, owing to the small size of the ducts, the change in point A has insignificance effect on the forces and therefore is considered a fixed point located at the intersection of the plane of the duct lip and z_d axis. For low speed operations the aerodynamic effects of the surfaces of the VTAV are negligible and therefore ignored.

3.4 Moments

The forces described in the previous section also generate moments about the center of gravity of the VTAV. Let $\overrightarrow{OS}$ be the distances between the center of gravity of the VTAV and the center of the duct on the x_b-y_b plane. Vertical distance from point S to center of propeller plane P and center of pressure A are measurable and are denoted by |SP| and |SA|.

If $\overrightarrow{OS} = [x_s \ y_s \ z_s]^T$ then $\overrightarrow{OP}$ and $\overrightarrow{OA}$ vectors can be derived as,

$$\overrightarrow{OP} = \overrightarrow{OS} + \overrightarrow{SP} = \begin{pmatrix} x_s \\ y_s \\ z_s \end{pmatrix} - \mid SP \mid \begin{pmatrix} s_{\theta_d} \\ 0 \\ c_{\theta_d} \end{pmatrix}, \quad (16)$$

$$\overrightarrow{OA} = \overrightarrow{OS} + \overrightarrow{SA} = \begin{pmatrix} x_s \\ y_s \\ z_s \end{pmatrix} - \mid SA \mid \begin{pmatrix} s_{\theta_d} \\ 0 \\ c_{\theta_d} \end{pmatrix}. \quad (17)$$

The matrix $(s_{\theta_d}, 0, c_{\theta_d})^T$ comes into play because of the vectoring of the fans. As discussed earlier cumulative F_{Tb} acts at propeller center P while F_{Db} acts at duct lip, A. Therefore the total moments acting on the VTAV body would be,

$$M_{Tb} = \overrightarrow{OP} \times F_{Tb}, \quad (18)$$

$$M_{Db} = \overrightarrow{OA} \times F_{Db}. \quad (19)$$

3.5 Dynamic Equations

The dynamic equatios of the VTAV can now be formed.

Let subscripts 1, 2 and 3 represent the front, right and left ducted fans of the VTAV, respectively. As the front ducted fan can not vector, θ_d=0. Distances SP and SA are same for all three fans. However the distance from the center of gravity to S_1, S_2 and S_3 vary as follows.

$$OS_1 = \begin{pmatrix} d & 0 & 0 \end{pmatrix}^T, \quad (20)$$

$$OS_2 = \begin{pmatrix} -e & f & 0 \end{pmatrix}^T, \quad (21)$$

$$OS_2 = \begin{pmatrix} -e & -f & 0 \end{pmatrix}^T. \quad (22)$$

The distance $d = 2e$. By using the force equations (6), (9) and (15), and the moment equations (18) and (19), the total forces and moments acting on the VTAV body are,

$$F_b = \sum_{j=1}^{3}(F_{Tb_j} + F_{Db_j}) + G_b, \quad (23)$$

$$M_b = \sum_{i=1}^{3}(M_{Tb_i} + M_{Db_i}). \quad (24)$$

The equations (23) and (24) represents the complete dynamic model of the system.

4 Linearized Hover Model

The result obtained in Section 3 yields that the modeled VTAV is a nonlinear, coupled, MIMO system. The VTAV dynamic model derived through Newton-Euler equations can be expressed as a set of first order nonlinear differential equations,

$$\dot{\mathbf{x}} = \mathbf{f}(\mathbf{x}, \mathbf{u}) \quad (25)$$

with the state vector $\mathbf{x}$ denoted by,

$$\mathbf{x} = \begin{pmatrix} v_{bx} & v_{by} & v_{bz} & \Phi & \Theta & \Psi & \omega_{bx} & \omega_{by} & \omega_{bz} \end{pmatrix}^{\mathbf{T}} \quad (26)$$

And the input vector $\mathbf{u}$ denoted by,

$$\mathbf{u} = \begin{pmatrix} \omega_{f_1} & \omega_{f_2} & \omega_{f_3} & \theta_{t_2} & \theta_{t_3} \end{pmatrix}^{\mathbf{T}} \quad (27)$$

This nonlinear VTAV model can be linearized around the hover condition where all the time derivatives and attitudes are zero (i. e. $\mathbf{x}_0 = 0_{9\times1}$) and the control input is such that the VTAV is hovering. As F_b=0 and M_b=0 at the hover equilibrium point, the corresponding input vector $\mathbf{u_0}$ can be expressed as,

$$\mathbf{u_0} = \begin{pmatrix} \omega_{f_{10}} & \omega_{f_{20}} & \omega_{f_{30}} & \theta_{t_{20}} & \theta_{t_{30}} \end{pmatrix}^{\mathbf{T}}, \quad (28)$$

where,

$$\theta_{t_{20}} = \theta_{t_{30}} = 0, \quad (29)$$

$$\omega_{f_{10}} = \sqrt{\frac{mge}{C_t(d+e)}}, \quad (30)$$

$$\omega_{f_{20}} = \sqrt{\frac{mgd}{C_t 2(d+e)}}, \quad (31)$$

$$\omega_{f_{20}} = \omega_{f_{30}}. \quad (32)$$

The linearized state space equation is obtained by substituting $\mathbf{x_0}$ and $\mathbf{u_0}$ to the Jacobian matrices in the following equation.

$$\delta\dot{\mathbf{x}} = \left(\frac{\partial \mathbf{f}}{\partial \mathbf{x}}\right)\Big|_{\mathbf{x_0},\mathbf{u_0}} \delta\mathbf{x} + \left(\frac{\partial \mathbf{f}}{\partial \mathbf{u}}\right)\Big|_{\mathbf{x_0},\mathbf{u_0}} \delta\mathbf{u} \quad (33)$$

The resulting linearized state space model can be expressed as,

$$\dot{\mathbf{x}} = \mathbf{A}\mathbf{x} + \mathbf{B}\mathbf{u} \quad (34)$$

$$\mathbf{y} = \mathbf{Cx} + \mathbf{Du} \tag{35}$$

The matrices **A, B, C** and **D** are,

$$\mathbf{A} = \begin{pmatrix} A_{11} & 0 & 0 & 0 & -g & 0 & 0 & 0 & 0 \\ 0 & A_{22} & 0 & g & 0 & 0 & 0 & 0 & 0 \\ 0 & 0 & 0 & 0 & 0 & 0 & 0 & 0 & 0 \\ 0 & 0 & 0 & 0 & 0 & 0 & 1 & 0 & 0 \\ 0 & 0 & 0 & 0 & 0 & 0 & 0 & 1 & 0 \\ 0 & 0 & 0 & 0 & 0 & 0 & 0 & 0 & 1 \\ 0 & A_{72} & 0 & 0 & 0 & 0 & 0 & 0 & 0 \\ A_{81} & 0 & 0 & 0 & 0 & 0 & 0 & 0 & 0 \\ 0 & A_{92} & 0 & 0 & 0 & 0 & 0 & 0 & 0 \end{pmatrix} \tag{36}$$

$$\mathbf{B} = \begin{pmatrix} 0 & 0 & 0 & B_{14} & B_{15} \\ 0 & 0 & 0 & 0 & 0 \\ B_{31} & B_{32} & B_{33} & 0 & 0 \\ 0 & 0 & 0 & 0 & 0 \\ 0 & 0 & 0 & 0 & 0 \\ 0 & 0 & 0 & 0 & 0 \\ 0 & B_{72} & B_{73} & 0 & 0 \\ B_{81} & B_{82} & B_{83} & 0 & 0 \\ 0 & 0 & 0 & B_{94} & B_{95} \end{pmatrix} \tag{37}$$

$$\mathbf{C} = \mathbf{I_{9\times 9}} \tag{38}$$

$$\mathbf{D} = \mathbf{0_{9\times 5}} \tag{39}$$

The elements of **A** and **B** matrices are shown in Table 1 and Table 2, respectively.

Table 1: Elements of Matrices A and B

$A_{11} = -C_d(\omega_{f10} + \omega_{f20} + \omega_{f30})/m$	$B_{33} = -2C_t\omega_{f30}/m$
$A_{22} = -C_d(\omega_{f10} + \omega_{f20} + \omega_{f30})/m$	$B_{72} = -2C_tf\omega_{f20}/I_{xx}$
$A_{72} = -C_d\|SA\|(\omega_{f10}+\omega_{f20}+\omega_{f30})/I_{xx}$	$B_{73} = 2C_tf\omega_{f30}/I_{xx}$
$A_{81} = C_d\|SA\|(\omega_{f10} + \omega_{f20} + \omega_{f30})/I_{yy}$	$B_{81} = 2C_td\omega_{f10}/I_{yy}$
$A_{92} = C_d(-d\omega_{f10} + e\omega_{f20} + e\omega_{f30})/I_{zz}$	$B_{82} = -2C_te\omega_{f20}/I_{yy}$
$B_{14} = -C_t\omega_{f20}^2/m$	$B_{83} = -2C_te\omega_{f30}/I_{yy}$
$B_{15} = -C_t\omega_{f30}^2/m$	$B_{94} = C_tf\omega_{f20}^2/I_{zz}$
$B_{31} = -2C_t\omega_{f10}/m$	$B_{95} = -C_tf\omega_{f30}^2/I_{zz}$
$B_{32} = -2C_t\omega_{f20}/m$	

Table 2: Nominal Values of VTAV Parameters

Parameter(unit)	Value	Parameter(unit)	Value
$m(kg)$	5.5	$I_{zz}(kgm^2)$	0.0917
$g(ms^{-2})$	9.81	$d(m)$	0.2310
C_t	0.0500	$e(m)$	0.1155
C_d	0.0005	$f(m)$	0.2000
C_m	0.0010	$\mid SP \mid (m)$	0.0050
$I_{xx}(kgm^2)$	0.0229	$\mid SA \mid (m)$	0.0250
$I_{yy}(kgm^2)$	0.1279		

5 Analysis of Linearized Hover Model

As discussed in Section 4 the system could be linearized at the hover equilibrium point. Although the system is linearized for simplicity, the derived linear model should behave similarly to the nonlinear system under the same set of control inputs, around hover condition in order to justify the linearization process. The aim of this section is to analyze the characteristics of the linearized VTAV model.

5.1 Stability

The stability of the dynamic model in response to inputs can be determined by evaluating the eigenvalues of the linearized system. The set of eigenvalues take the following form.

$$\sigma_A = [0, 0, 0, f_4, f_5, f_6, f_7, f_8, f_9]^T \tag{40}$$

where f_4 to f_9 are functions of I_{xx} , I_{yy}, I_{zz}, m, g, |SA|, |SP|, d, e, f, C_t and C_d. The symbolic expressions for f_4 to f_9 are not presented for brevity. By substituting numerical values, the eigenvalues can be obtained as,

$$\sigma_A = \begin{pmatrix} 0 \\ 0 \\ 0 \\ -0.2589 \\ 0.1286 + 0.2238i \\ 0.1286 - 0.2238i \\ -0.4590 \\ 0.2287 + 0.3970i \\ 0.2287 - 0.3970i \end{pmatrix} \tag{41}$$

It can be clearly seen that four of the eigenvalues strictly lie on the right hand side of the complex plane. Therefore, according to Lyapanov's linearization theorem, the VTAV model has an unstable equilibrium point [Slotine and Li, 1991]. This result suggests that the system is unable to return to stable hover if subjected to perturbations. The triple poles at the origin as shown in (40) are independent of the system parameters and hence the system cannot be made to be any stable by choosing the system's design parameters.

5.2 Controllability

Before developing a controller for the VTAV it is important to check whether the system is controllable. The controllability of the system could be determined by evaluating the rank of the controllability matrix shown in (42).

$$\mathcal{C} = [\mathbf{B} \;\; \mathbf{AB} \;\; \mathbf{A^2B} \;\; \ldots \;\; \mathbf{A^{n-1}B}] \tag{42}$$

Noting that the linearized system has nine states and, when evaluated, the rank of the matrix in (42) is nine, the system is fully controllable.

5.3 Frequency Response

The relationship between the linearized system inputs and outputs can be further analyzed by converting the existing state space equation to a s-plane transfer function. The transfer function can be obtained from the state space system through the following equation.

$$G(s) = \mathbf{C(sI - A)^{-1}B} \tag{43}$$

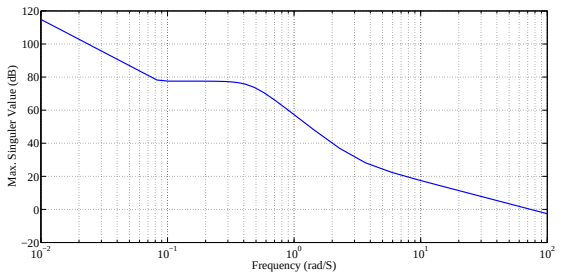

Figure 4: Frequency response of Maximum Singuler Value of the System

The transfer function $G(s)$ can be used to obtain the frequency response of the system which helps in determining the bandwidth of a controlled system. The frequency response of the system could be analyzed by substituting s with $j\omega$, where ω is the frequency. The maximum singular value of the system $\bar{\sigma}(G(0))$ and its frequency response gives the operable bandwidth, ω_c, of the linearized model [Skogested and Postlethwaite, 2001]. The frequency response of the maximum singular value for the linearized VTAV model is shown in Figure. 4. However the bandwidth ω_c could be further limited by the actuator dynamics $G_a(s)$ which represents the transfer function between the input signal and the fan speed ω_f. Generally $G_a(s)$ takes the form,

$$G_a = \frac{A_a}{1+\tau s} \tag{44}$$

where A_a is the actuator gain and τ is the time constant of the motor and is considered very small in this case.

6 System Response

The dynamic response of the linearized VTAV model was analyzed with respect to the nonlinear VTAV model for various test conditions. As discussed in Section 4 when ω_{f1}=ω_{f2}=ω_{f3}=5.997 rad/s and θ_{t2}=θ_{t3}=0 the system is in hover condition. In the cases where ω_{f1}=ω_{f2}=ω_{f3} $\neq$ 5.997 rad/s and θ_{t2}=θ_{t3}=0 the system becomes unstable in the direction of z_b axis but this unstable condition can in fact be used to maneuver the VTAV vertically in space. For example, the operator will be able to control the VTAV in z_b direction by increasing/decreasing speeds of all three ducted fans equally. Figures 5-8 illustrates this in which the vertical translation of the VTAV is achieved while keeping the attitude dynamics in equilibrium for both nonlinear and linear models. Note that the VTAV is in equilibrium initially, and the speeds of the fans are increased at t = 2S. To achieve this, the following two conditions should be maintained.

- ω_{f1}=ω_{f2}=ω_{f3}
- θ_{t2}=θ_{t3}=0

However this is not the case in real-world scenarios. Various types of disturbances interfere with the system and will jolt the system out of its equilibrium point. In order to observe the effect of disturbances on the linearized VTAV model, a disturbance signal in the form of an impulse was applied to one of the rear fans of the vehicle, while the system was operating in the hover condition. As illustrated by Figure 10, the applied impulse triggers a roll movement and later a pitch movement of the VTAV and as expected was unable to return to stable equilibrium at the end of the impulse disturbance. Instead the system becomes unstable and started to spiral continuously as shown in Figure 11. Note that the initial position is denoted as A. The non linear system too became unstable for the same impulse as shown in Figure 14, suggesting that the unstable behavior is the effect of system parameters of the VTAV rather than linearization. However, the nonlinear model reacts slower than the linearized model in in response to the impulse.

The effect of wind gusts were also investigated. The behavior of the nonlinear model in the presence of wind gusts, clearly indicates that the slightest airflow with respect to the body could affect the operation of the vehicle adversely as shown in Figure 16. On the other hand, the linearized system model which does not contain any parameters related to relative motion of air with respect to the VTAV body, does not exhibit any variation from the hover condition in the simulation environment. Clearly this does not hold true for the real system. Therefore, when developing a controller for the linearized model a suitable wind model should be added to the system in order to acquire desired performances.

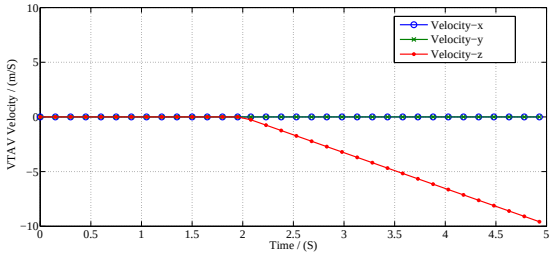

Figure 5: Velocities of linear model with increased fan speeds

7 Conclusion

This paper presented a comprehensive dynamic model of the VTAV. The model is simpler than that of a helicopter thereby significantly simplifying the future development of controllers. It was also shown that the system is in unstable equilibrium. Due to the existence of poles at the origin, which cannot be influenced by the system parameters, the VTAV's design does not allow it to be converted to a system that operates in

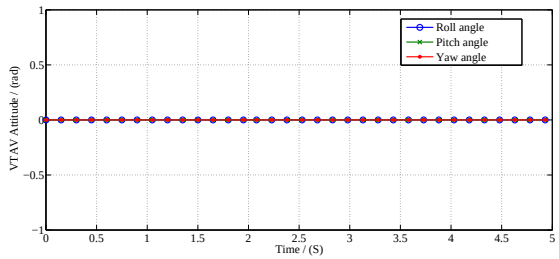

Figure 6: Attitude of linear model with increased fan speeds

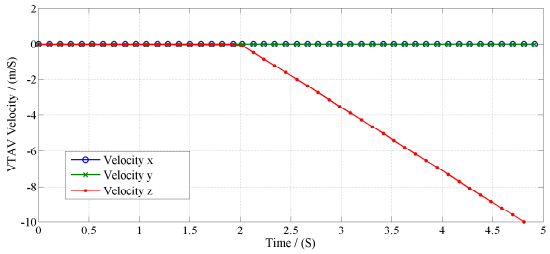

Figure 7: Velocities of nonlinear model with increased fan speeds

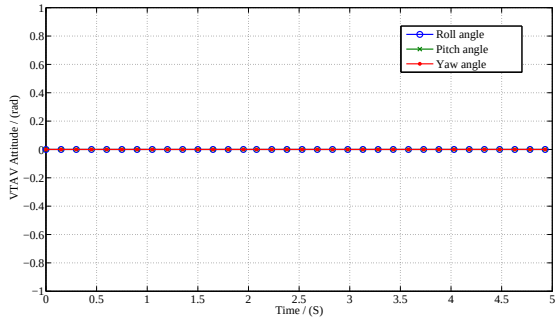

Figure 8: Attitude of nonlinear model with increased fan speeds

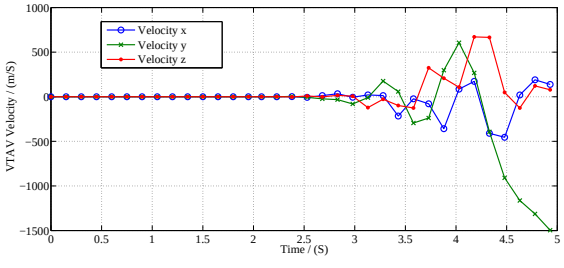

Figure 9: Velocity response of linear model under impulse disturbance

stable equilibrium. This, however, is an advantage in achieving better maneuverability in controlled flight. Although the linearized model behaves similarly to the nonlinear model in the near hover condition, it

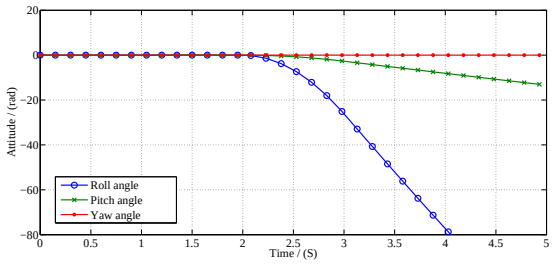

Figure 10: Attitude response of linear model under a sudden disturbance

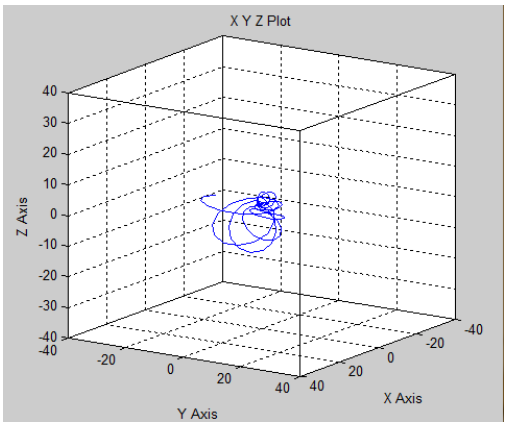

Figure 11: Translation of linear model under impulse disturbance

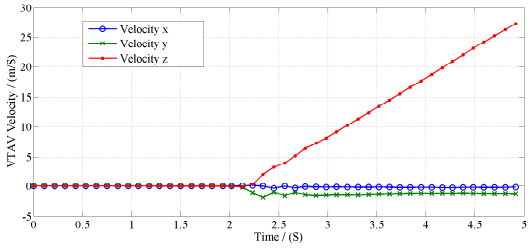

Figure 12: Velocity response of nonlinear model under impulse disturbance

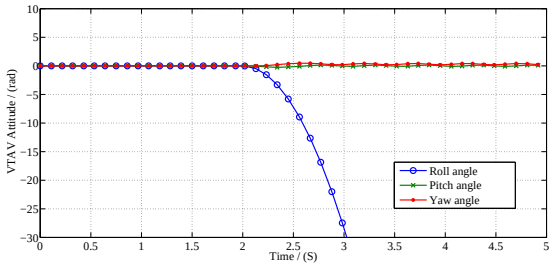

Figure 13: Attitude response of nonlinear model under impulse disturbance

is unable to respond to the effect of wind owing to the fact that the forces related to relative motion of air

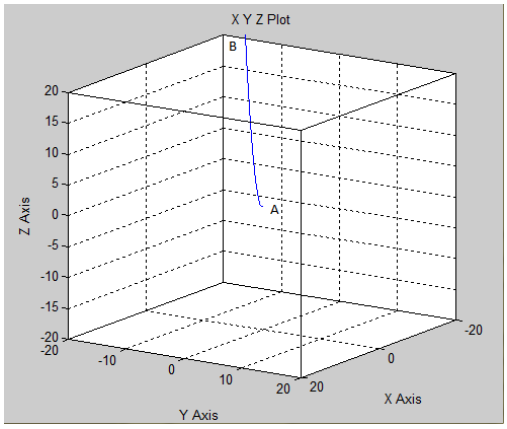

Figure 14: Translation of nonlinear model under impulse disturbance

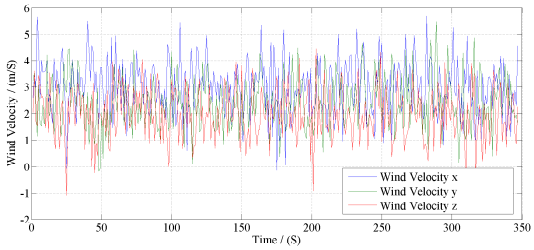

Figure 15: Wind disturbance applied to nonlinear model

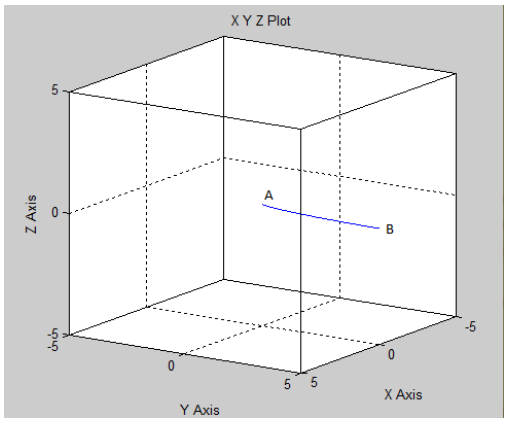

Figure 16: Translation of nonlinear model under wind disturbances

with respect to the VTAV have been eliminated in the linearization process. Apart from that both systems, having unstable equilibrium point, are vulnerable to disturbances when not being controlled.

References

[Bai *et al.*, 2011] Yue Bai, Xun Gong, Zhicheng Hou, and Yantao Tian. Stability control of quad-rotor based on explicit model following with inverse model feedforward method. pages 2189 – 2194, 2011.

[Johnson and Turbe, 2006] Eric N. Johnson and Michael A. Turbe. Modeling, control, and flight testing of a small ducted-fan aircraft. *Journal of Guidance, Control, and Dynamics*, 29(4):769 – 779, 2006.

[Ko *et al.*, 2007] Andy Ko, John Ohanian, and Paul Gelhausen. Ducted fan uav modeling and simulation in preliminary design. 2007.

[Kumon *et al.*, 2010] Makoto Kumon, Hugh Cover, and Jayantha Katupitiya. Hovering control of vectored thrust aerial vehicles. pages 1149 – 1154, 2010.

[Liu *et al.*, 2009] Xiaojie Liu, Xiaohui Zhao, Haijun Gu, and Anand Sanchez. Application and design of real-time control system for the quad-rotor helicopter. volume 2, pages 40 – 44, 2009.

[Marconi *et al.*, 2011] Lorenzo Marconi, Roberto Naldi, and Luca Gentili. Modelling and control of a flying robot interacting with the environment. *Automatica*, 47(12):2571 – 2583, 2011.

[Naldi *et al.*, 2010] Roberto Naldi, Luca Gentili, Lorenzo Marconi, and Andrea Sala. Design and experimental validation of a nonlinear control law for a ducted-fan miniature aerial vehicle. *Control Engineering Practice*, 18(7):747 – 760, 2010.

[Omar *et al.*, 2008] Zamri Omar, Cees Bil, and Robin Hill. The application of fuzzy logic on transition manoeuvre control of a new ducted-fan vtol uav configuration. Kumamoto, Japan, 2008.

[Pflimlin *et al.*, 2010] J.-M. Pflimlin, P. Binetti, P. Soueres, T. Hamel, and D. Trouchet. Modeling and attitude control analysis of a ducted-fan micro aerial vehicle. *Control Engineering Practice*, 18(3):209 – 218, 2010.

[Skogested and Postlethwaite, 2001] Sigurd Skogested and Ian Postlethwaite. Multivariable feedback control analysis and design. *John Wiley and Sons*, 2001.

[Slotine and Li, 1991] J.J.E. Slotine and W. Li. *Applied nonlinear control*. Prentice Hall, 1 edition, 1991.

[Wang *et al.*, 2007] Hongqiang Wang, Daobo Wang, Xinwen Niu, and Haibin Duan. Modeling and hover control of a novel unmanned coaxial rotor/ducted-fan helicopter. pages 1768 – 1773, 2007.